Number Density of Turbulent Vortices in the Entire Energy Spectrum

AIChE

Number Density of Turbulent Vortices in the Entire Energy Spectrum

Farideh Ghasempour, Ronnie Andersson, and Bengt Andersson
Dept. of Chemical and Biological Engineering, Chalmers University of Technology, SE-412 96, Gothenburg, Sweden

Donald J. Bergstrom
Dept. of Mechanical Engineering, University of Saskatchewan, S7N 5A9, Saskatoon, Canada

DOI 10.1002/aic.14622
Published online September 16, 2014 in Wiley Online Library (wileyonlinelibrary.com)

In coalescence and break-up modeling, vortex number density and size distributions of turbulent vortices are required to calculate the rate of interaction between continuous and dispersed phases. Existing number density models are only valid for the inertial subrange of the energy spectrum and no model of the vortex number density, valid for the entire energy spectrum, is available. The number density of the turbulent vortices were studied and modeled for the entire energy spectrum including the dissipative, inertial, and energy containing subranges. It was observed that the new number density model depends on vortex size, local turbulent kinetic energy, and dissipation rate. Moreover, the new number density model was validated by the number density distributions quantified in a turbulent pipe flow. The turbulent vortices of the pipe were identified and labeled using a vortex-tracking algorithm that was developed recently by the authors. © 2014 The Authors AIChE Journal published by Wiley Periodicals, Inc. on behalf of American Institute of Chemical Engineers *AIChE J*, 60: 3989–3995, 2014
Keywords: number density, vortex size, vortex-tracking algorithm, LES

Introduction

Mixing, coalescence, and break-up of fluid particles are common phenomena in reactors and separation units in chemical engineering industries. These phenomena are significantly influenced by the turbulence in the continuous phase. A detailed description of the turbulence in the continuous phase helps to understand and make quantitative prediction of mixing, coalescence, and break-up phenomena in chemical engineering processes. The detailed description of turbulence includes the properties of single turbulent vortices such as vortex size, number density, growth rate, energy, and vorticity. To date, this issue has not been addressed adequately for three-dimensional (3-D) vortices in the entire energy spectrum.

As a matter of fact, coalescence and break-up of fluid particles result from interactions between fluid particle and single or paired turbulent vortices in the continuous phase.[1,2] The interaction rate and fluid particle break-up frequencies are calculated from the number density distribution of turbulent vortices in the size range of interest.[2,3] The number density of the turbulent vortices is the number of turbulent vortices per unit fluid volume. Besides, the interaction rate depends on the size distribution of turbulent vortices of the continuous phase. The turbulent vortices of interest are considered to be close in size or somewhat larger than the fluid particles sizes.[4] Very large vortices simply transport the fluid particle without causing break-up or collision, while very small vortices do not contain sufficient energy to affect the fluid particle.

Existing models of vortex number density implemented in break-up and coalescence models are valid only for the inertial subrange. Recently, available models on vortex number density in the inertial subrange of energy spectrum were studied by the authors.[5]

In fact, the Taylor microscale Reynolds number should be very large, at least more than 100, to have a noticeable inertial subrange in the turbulent energy spectrum.[6] However, large Taylor microscale Reynolds numbers are rarely obtained in chemical process equipment. Therefore, it is very important to model the vortex number density for a wider range of the turbulent energy spectrum. Unfortunately, no model for vortex number density is available which is valid for a wider range of flow situations. For these reasons, studies on vortex number density for entire energy spectrum including the different subranges of the spectrum are required as a foundation for further investigations.

The objective of the present study is to determine the number density of turbulent vortices for a complete energy spectrum including the dissipation, inertial, and energy containing subranges of the spectrum. In this study, models on the vortex number density for the three different subranges and the entire range of the energy spectrum were derived separately. The turbulent vortices in pipe flow were also identified by a 3-D vortex-tracking algorithm recently developed by the authors(Ghasempour et al., Submitted). The 3-D vortex-tracking algorithm identifies, quantifies, and tracks individual 3-D turbulent vortices in space and time. In the

Correspondence concerning this article should be addressed to F. Ghasempour at farideh@chalmers.se, ghasempour.frd@gmail.com.

next step, vortex number density distributions predicted by the models were validated using the number density distributions obtained by the vortex-tracking algorithm. Additionally, the vortex number density was studied at different radial locations and local turbulent properties. Finally, the vortex size distributions were described as a function of their locations.

Number Density of Turbulent Vortices

The number density of turbulent vortices can be formulated by writing an energy balance for vortices of sizes ranging from λ to $\lambda + d\lambda$, equivalent to wave number between κ and $\kappa + d\kappa$, where the wave number, κ, is $2\pi/\lambda$. The energy spectrum, $E(\kappa)$, gives the turbulent kinetic energy within in the vortices of wave number between κ and $\kappa + d\kappa$ per unit mass

$$\dot{n}_\lambda \rho_c \frac{\pi}{6}\lambda^3 \frac{\overline{u}_\lambda^2}{2} d\lambda = E_{\text{spectrum}}(\kappa)\rho_c(-d\kappa) \tag{1}$$

where $\bar{u}_\lambda$ (Eq. 2) is the mean fluctuating velocity of turbulent vortices of size λ. Number density of vortices, $\dot{n}$, can be calculated by integrating Eq. 1.

Some studies have been found about the number density of turbulent vortices; however, the proposed models are valid only in the inertial subrange of the energy spectrum. For isotropic turbulence, in which the vortex size of interest lies in the inertial subrange, the energy spectrum decays according to the $-5/3$ law. Moreover, the mean fluctuating velocity of turbulent vortices of size λ is theoretically given by[7]

$$\bar{u}_\lambda \approx C^{1/2}(\varepsilon\lambda)^{1/3} \tag{2}$$

where C is the functional parameter of the turbulent structure.

Azbel and Athanasios[8] defined a model for number density of vortices that decays with wave number κ per mass of fluid. Prince and Blanch[3] pointed out that Azbel and Athanasios model gives infinitely large numbers as the vortex size approaches very small vortices. To avoid this problem, they arbitrarily selected a minimum vortex size. In another study, Dritschel[9] studied the vortex number density of an unforced two-dimensional turbulent flow as a function of vortex area. Luo and Svendsen,[10] Jakobsen,[7] and Han et al.[11] showed that the vortex number density in the inertial subrange decays with the vortex size by the slope of -3. Han et al.[11] investigated the influence of complete energy spectrum on drop breakage in turbulent flow, however, the number density model that they formulated is valid only for the inertial subrange. Recently, the slope -3 was confirmed by the authors for number density of turbulent vortices quantified also in a rather low Reynolds number turbulent flow.[5] In the study, different offsets were found for the vortex number density distributions. The offsets were derived from the functional parameter of the turbulent structure, C, in the mean fluctuating velocity of turbulent vortices (Eq. 2). A number of studies reported very different estimates for C.[5–7,10,12,13] It was also concluded that the calculated number densities for vortices in the inertial subrange of a turbulent pipe flow are in good agreement with the models including the coefficient from Batchelor[12] and Martinez-Bazan et al.[13] studies.

As discussed earlier, all aforementioned models are valid for vortex sizes in the inertial subrange; however, the entire turbulent spectrum is of interest in this article. To find the number density of turbulent vortices for the entire spectrum of the vortex size, the complete turbulent energy spectrum must be considered. The complete turbulent energy spectrum for the entire vortex size range is given by[6]

$$E(\kappa) = \alpha\varepsilon^{2/3}\kappa^{-5/3} f_L(\kappa L) f_\eta(\kappa\eta) \tag{3}$$

where f_L and f_η are the nondimensional functions to determine the shape of the energy containing and dissipation ranges in the energy spectrum. The f_L and f_η functions are

$$f_L(\kappa L) = \left(\frac{\kappa L}{\left[(\kappa L)^2 + C_L\right]^{1/2}}\right)^{\frac{5}{3}+P_0} \tag{4}$$

$$f_\eta(\kappa\eta) = \exp\left\{-\beta\left\{\left[(\kappa\eta)^4 + C_\eta^4\right]^{1/4} - C_\eta\right\}\right\} \tag{5}$$

C_L, C_η, P_0, α, and β are the constants that are equal to 6.78, 0.4, 2, 1.5, and 5.2, respectively. Moreover, L and η are the turbulent large and Kolmogorov scales that are defined by

$$L \equiv \frac{k^{3/2}}{\varepsilon} \tag{6}$$

$$\eta = \left(\frac{\upsilon^3}{\varepsilon}\right)^{1/4} \tag{7}$$

where υ, ε, and k are kinematic viscosity, dissipation rate, and turbulent kinetic energy, respectively. To formulate the energy balance and calculate the number density for the entire energy spectrum, the mean fluctuating velocity, $\bar{u}_\lambda$, is also required for the entire energy spectrum. Generally, $\bar{u}_\lambda$ given by Eq. 2 is written for the vortices in the inertial subrange; however, it can also be used for the entire energy spectrum.[6] The overall kinetic energy production is equal to the dissipation rate, and it is reasonable to assume that the kinetic energy supply rate from the large turbulence scales to the small ones is related to the time scale of the large vortices. Therefore, the dissipation rate can be estimated by the correlation of $\varepsilon \approx \bar{u}_\lambda^3/\lambda$.

Computing the turbulent flow properties by Eqs. 6 and 7, and substituting Eqs. 2–5 into Eq. 1, the number density of turbulent vortices of sizes between λ and $\lambda + d\lambda$ can be calculated. Implementing the models of the turbulent energy spectrum for different subranges gives different number density equations. Based on the turbulent energy spectrum implemented, the number densities are summarized in Table 1. It should be noted that the number densities of turbulent vortices can be calculated by integrating of the models in Table 1.

Methodology

Large eddy simulation

In this research work, turbulence was modeled using large eddy simulation (LES) with the dynamic Smagorinsky–Lilly subgrid scale model. The simulation was performed for turbulent flow a straight pipe with 5 cm in diameter and 20 cm in length. The fluid in the pipe was water at Reynolds number of 20,000, resulting in an average Taylor microscale Reynolds number of 80. As shown in Figure 1, the computational domain consisted of two regions: one region had an overall fine grid and the other region contained a denser grid. The denser region covered the domain from near wall to the bulk of the flow, and it was constructed to minimize the total number of cells. The analysis was carried out in the

Table 1. Number Density Models for Different Energy Spectrum Subranges

Model	Subrange
$\dot{n}_\lambda = \frac{24\alpha}{C(2\pi)^{5/3}} \lambda^{-4} f_\eta$	Dissipation subrange
$\dot{n}_\lambda = \frac{24\alpha}{C(2\pi)^{5/3}} \lambda^{-4} f_L$	Energy containing subrange
$\dot{n}_\lambda = \frac{24\alpha}{C(2\pi)^{5/3}} \lambda^{-4}$	Inertial subrange
$\dot{n}_\lambda = \frac{24\alpha}{C(2\pi)^{5/3}} f_L f_\eta \lambda^{-4}$	Complete energy spectrum

denser region including of 248 × 138 × 572 cells in height, width, and flow direction, respectively. In total, the computational domain yielded a total number of 17 million cells. The cell sizes were smaller than the Taylor microscale sizes at Reynolds number of 20,000.

The quality of the LES simulation in the denser region was evaluated using the ratio of the resolved turbulent kinetic energy to the total one, the ratio of sub-grid scale (SGS) turbulent viscosity to the molecular viscosity, two-point correlations of velocities, and the y^+ value. In addition, a mesh convergence study was carried out for two different mesh resolutions in order to assure the quality of the LES simulations.

The ratio of the resolved turbulent kinetic energy to the total energy was more than 95%. When 80% of the turbulent kinetic energy is resolved, the LES simulation is considered well resolved.[14] At least 5–10 cells are required to indicate that the largest scales are well resolved in LES data.[15] A two-point correlation analysis further showed that the minimum number of cells resolving the large scales in the flow axis directions (x, y, and z) were 11, 7, and 15. In these simulations at $y^+ < 6$, the instantaneous subgrid turbulent viscosity ratio was lower than 0.015 and the maximum of this ratio in the whole denser region was 0.05. Besides, the maximum and mean instantaneous wall y^+ were 0.7 and 0.4. As turbulent kinetic energy and SGS turbulent viscosity ratios, grid resolutions, and y^+ values were all within the accepted range, the LES simulations are considered well resolved.

Mesh convergence study results for two different mesh resolutions show a minor difference in the root mean square (RMS) velocities which is somewhat higher close to the wall, as expected, as a larger part of the turbulent kinetic energy is resolved with finer mesh. A power spectra in axial direction at the center of the pipe showed that a lower range for the inertial subrange is 2 mm at $Re = 20{,}000$.[5]

3-D vortex-tracking algorithm

Previously, different methods for vortex identifying, characterizing and tracking have been developed by the authors.[5,16] The latest developed method was a 3-D vortex-tracking algorithm used to identify, quantify, and track individual 3-D turbulent vortices using morphological methods (Ghasempour et al., Submitted). In the 3-D vortex-tracking algorithm, the normalized Q-criterion was used to identify the turbulent vortex cores. To provide a good balance that allows capturing as many as possible cores of the turbulent vortices, but leaves out most of the incoherent normalized Q-criterion, 0.1 was selected as the threshold. The data were resampled onto an equidistant Cartesian grid in MATLAB, and in the next step, Gaussian smoothing operator was used to restrain the image noises. The visualization of turbulent vortices was improved using mathematical morphological techniques. The morphological techniques called "opening-by-reconstruction" and "closing-by-reconstruction" were used to clean-up the images. Turbulent structure containing less than five grid-cells were removed in order to obtain a stable algorithm, that is, only turbulent core structures larger than about 0.4 mm were kept.

Morphological image segmentation algorithms such as marker-controlled watershed and region growing and watershed merging algorithms were applied to identify and extract the individual turbulent vortex. The segmented regions were labeled with unique numbers. These labeled vortices, which are vortex-cores, contained less than 27% of total turbulent kinetic energy and a larger fraction of the turbulent kinetic energy related to the vortex is located outside the vortex core. To increase the amount of energy captured within the vortices, their volumes must be extended. Different methods were used to extend volume of the vortices (Ghasempour et al., Submitted).[5] In this algorithm, turbulent vortices were regrowing using distance transform to increase the amount of turbulent kinetic energy captured. The regrown vortices contained more than 80% of the total turbulent kinetic energy. Finally, the properties within each extended vortex containing unique label were integrated over the volume of the vortex to obtain the corresponding turbulent vortex data. In the algorithm, the regrown vortices describe the real shape/volume of turbulent vortices.

In the present study, the 3-D vortex-tracking algorithm was implemented for identification of turbulent vortices in the denser region of the computational domain at one time step. The number density models formulated for different subranges separately (dissipation, inertial, and energy containing subranges) and the entire energy spectrum (Table 1) were studied and compared with the number density distributions of turbulent vortices, before and after regrowing process in the vortex-tracking algorithm. The range of vortex sizes includes all turbulent vortices between the smallest and largest vortex sizes identified using the algorithm. The spherical equivalent diameter of the vortex was considered as the

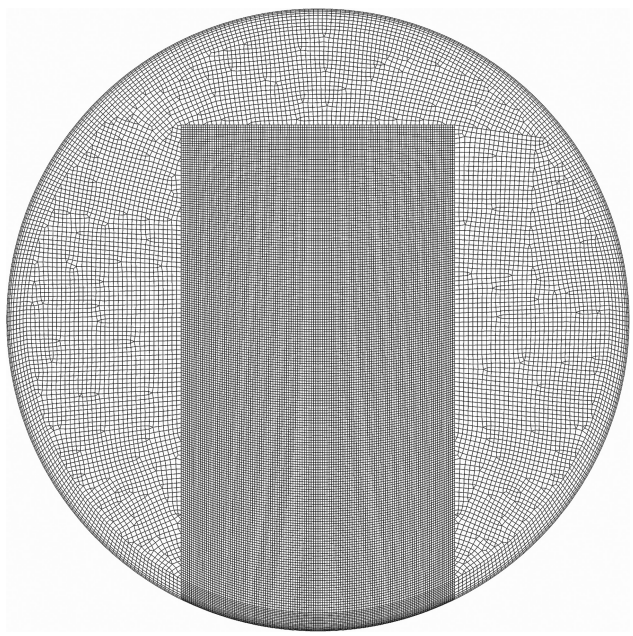

Figure 1. Grids of a cutting-plane in the pipe.

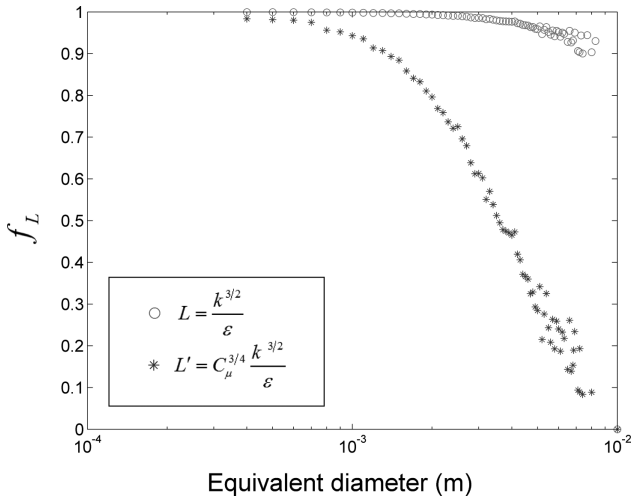

Figure 2. Variation of f_L with respect to equivalent diameter of vortices.

[Color figure can be viewed in the online issue, which is available at wileyonlinelibrary.com.]

vortex size. Moreover, the number density distributions of turbulent vortices were studied at six different radial fractions in the denser region of the pipe. In this study, the regrown vortices were considered as the turbulent vortices with real volume and the major studies were performed on them.

Results and Discussion

Studies on the number density model formulated for the dissipation subrange of the energy spectrum showed that the function f_η forms the number density for the turbulent vortices in the related subrange. Furthermore, as expected, the number density model for the inertial subrange decays linearly respect to the vortex size with the slope of -3. However, it was found that the function f_L together with Eq. 6 for turbulent large scales in the energy containing model (Table 1), does not form the number density of the corresponding subrange.

The function f_L which depends on the turbulent large scales was studied to investigate the influence of this function on forming of the energy spectrum. f_L varies between 0 and 1 for energy containing vortices; however, it is unity for the inertial subrange. As shown in Figure 2, the f_L together with $L=\frac{k^{3/2}}{\varepsilon}$ is barely smaller than unity for large vortices. Therefore, f_L has little influence on the number density model even in the energy containing subrange. Another alternative estimation for turbulent large scales is $L'=C_\mu^{3/4}\frac{k^{3/2}}{\varepsilon}$.[17] Here, C_μ is a universal constant which is equal to 0.09. It should be noted that Eq. 6 is the well-known Prandtl–Kolmogorov relation, which uses the constant C_μ to determine the energy containing length scale. It was found that L' strongly affects the function f_L. Equation 6 gives the largest length scale compared to L'; however, both L and L' profiles are similar. It should be noted that L' confirmed reasonably according to the two-point correlation analysis. In this study, L' was used.

Figures 3a–c show the number density models for dissipation, inertial, and energy containing subranges of the energy spectrum vs. the vortex size. Considering the fact that it is difficult to find accurate boundaries for the dissipative, inertial, and energy containing subranges in any energy spectrum, it is worth to study the number density model for the entire energy spectrum that covers entire range of the vortex size. The new number density model obtained for the entire energy spectrum is shown in Figure 3d and compared with the traditional number density model for the inertial subrange (Table 1). Our previous study[5] showed that the number density model for the inertial subrange has different offsets. It was also concluded that the best fitted offset is computed from Batchelor[12] and Martinez-Bazan[13] coefficients. Here in this study, the number density model including the coefficient from Batchelor[12] and Martinez-Bazan et al.[13] studies was considered as the traditional/old number density model for the comparison. It should be noted that the very recent number density model obtained by Han et al.[11] gives number density distribution four times larger than the old model (Figure 3d, dash dotted line). Figure 3 shows that the old/traditional number density model for the inertial subrange overestimates the number of turbulent vortices in the dissipation and energy containing subranges, whereas the agreement in the inertial subrange is good.

The constants in the new number density model were selected based on what Pope[6] has suggested; however, other alternative constants such as α (1.5 and 1.62 [11]) and P_0 (2 and 4 [6]) were studied in order to investigate the uncertainties of resulting number density profile. It was found that number density profiles deviations are smaller than 4% in the inertial subrange and 10% in the energy containing subrange.

In Figure 4, number density distribution of the turbulent vortex-cores (before regrowing process in the 3-D vortex-tracking algorithm) with respect to the size is presented. The traditional and new number density models are also plotted in Figure 4. The figure illustrates that the old number density model overestimates the number density of turbulent vortices in the dissipation and energy containing subranges; however, the new number density model for the entire energy spectrum predicts more reliable number densities for the dissipation and energy containing subranges. It should be noted that

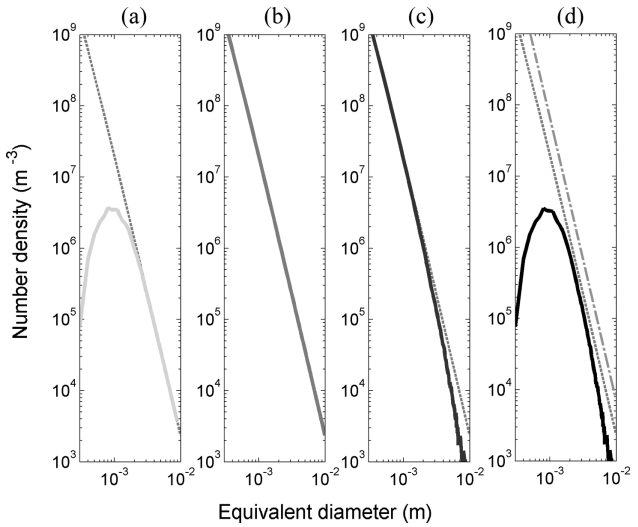

Figure 3. Number density models for: (a) dissipation, (b) inertial, (c) energy containing, and (d) solid line: complete energy spectrum and dash dotted line: Han et al.[11] model.

The dashed lines are traditional number density model. [Color figure can be viewed in the online issue, which is available at wileyonlinelibrary.com.]

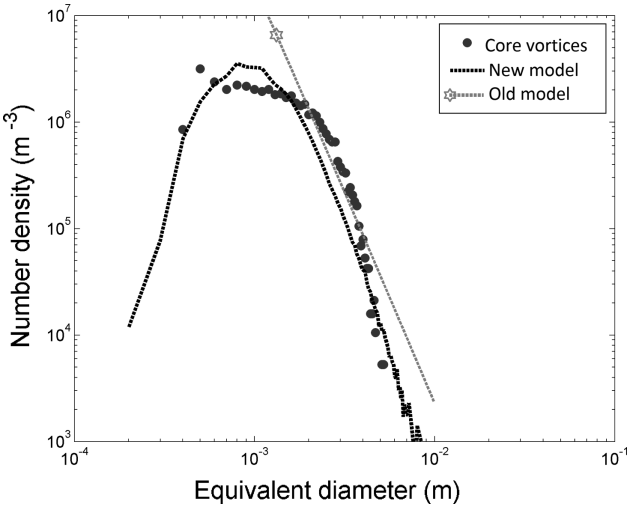

Figure 4. Number density distribution of turbulent vortex-cores quantified using the vortex-tracking algorithm.

The new and old models are dashed lines with different colors. [Color figure can be viewed in the online issue, which is available at wileyonlinelibrary.com.]

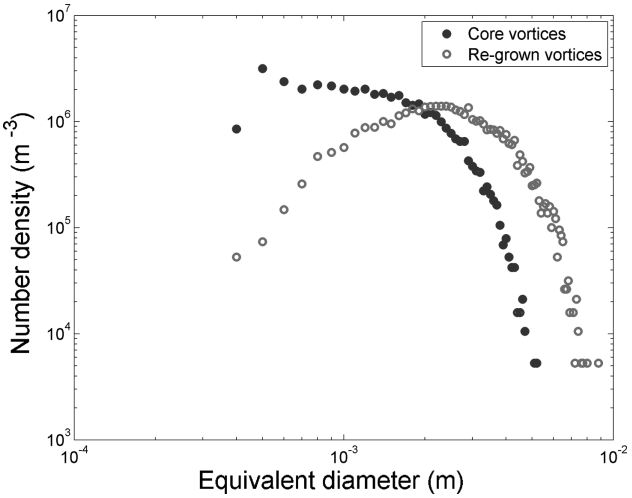

Figure 5. Number density distributions of vortex cores and regrown vortices identified using the vortex-tracking algorithm.

[Color figure can be viewed in the online issue, which is available at wileyonlinelibrary.com.]

the number of turbulent vortices in the dissipation subrange depends on the LES resolution, and in the 3-D vortex-tracking algorithm, all vortex-cores containing less than five grid cells result in a minimum size of about 0.4 mm were removed. As discussed in the algorithm, the vortex-cores only capture a fraction of available turbulent kinetic energy; however, the regrown vortices capture most of the energy. Therefore, the study on the regrown vortices is of interest.

The number density of regrown turbulent vortices was studied to evaluate the influence of regrowing process in the vortex-tracking algorithm, which was performed to increase the amount of captured energy within each individual vortex. Both number densities of turbulent vortex-cores and regrown vortices are shown in Figure 5. Overall, the number density distributions of vortex-cores and regrown vortices are similar. They both show number densities decay for relevant vortex sizes in the inertial subrange and larger. However, there is a shift in equivalent diameter of vortices due to the regrowing process of the vortex-cores in the algorithm. This main difference is seen for small vortices. The vortex-tracking algorithm regrows vortex-cores based on their proximity to other vortices and vorticity magnitudes. As the small vortex-cores are generally located in the near-wall region in which the vorticity magnitudes are high, they regrow more. The regrowing process of the 3-D vortex-tracking algorithm makes the entire range of the vortex sizes wider. Whereas, regrowing process increases the number of turbulent vortices in the inertial subrange, it does not influence the total number of turbulent vortices in the computational domain.

Figure 6 provides a comparison between the quantified number density distribution of the regrown turbulent vortices and the new number density model. As shown in Figure 6, the overall distributions of the quantified number densities and the model for the entire energy spectrum are similar. As earlier mentioned, all core vortices below 0.4 mm in size were removed in the vortex-tracking algorithm. Consequently, these vortices that after regrowing would be above 0.4 mm have been removed. As regrowing increases the average size of the vortices with a factor 1.5–2 and somewhat larger close to the wall there will be too few detected vortices below 1.5 mm. In Figure 6, the number density model for the entire vortex size spectrum was shifted by 1.8 (this is an average factor that turbulent vortex-cores were regrown).

In Figure 7, the number density of turbulent vortices predicted with the new model at different radial locations are shown. The new number density model for the entire energy spectrum depends on the local turbulent kinetic energy and dissipation rate. As the turbulent kinetic energy and dissipation rate are varying with the pipe radius and most of the variations are in areas with high shear rate close to the wall (i.e., $0.93 < r/R < 1$ and $y^+ < 30$), it was highly motivated to do the analysis also at different radial locations. It was found that the number density models of turbulent vortices vary at different radial locations. The difference is more evident for

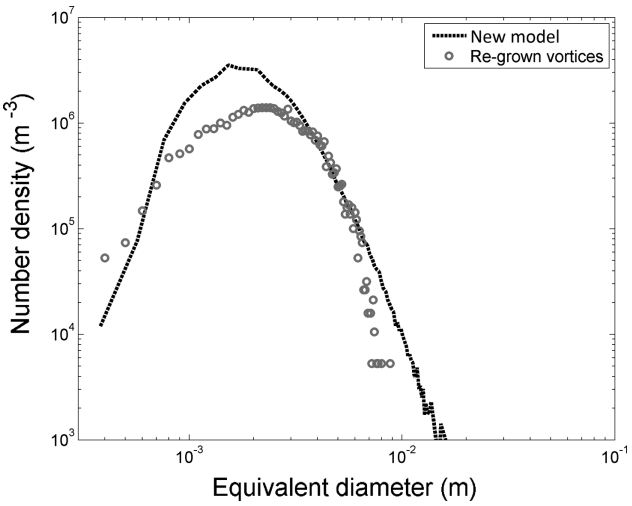

Figure 6. Number density distribution of turbulent vortices (regrown vortices) quantified using the vortex-tracking algorithm.

The new model is the dashed line. [Color figure can be viewed in the online issue, which is available at wileyonlinelibrary.com.]

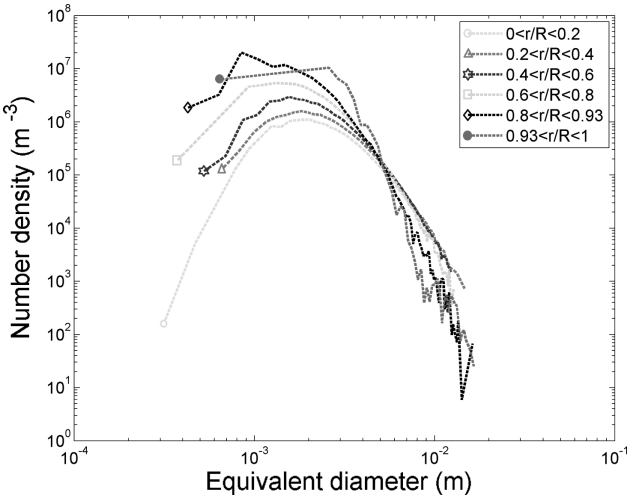

Figure 7. Number density of turbulent vortices predicted with the new model at different radial locations.

[Color figure can be viewed in the online issue, which is available at wileyonlinelibrary.com.]

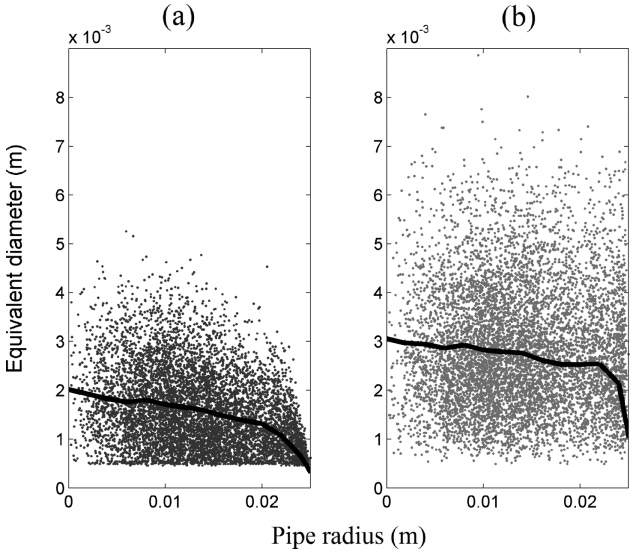

Figure 9. (a) Size distributions of vortex-cores and (b) size distributions of regrown vortices identified using the vortex-tracking algorithm with respect to the pipe radius.

[Color figure can be viewed in the online issue, which is available at wileyonlinelibrary.com.]

the near-wall regions. Some number density predictions in Figure 7 are not smooth due to averaging the turbulent properties. Moreover, the turbulent vortices of equal size are radially spread in the entire computational domain.

A comparison between the number density distributions predicted with the new model and vortex-tracking algorithm at different radial locations is shown in Figure 8. As shown in Figure 8, the highest number density is for the near-wall region ($y^+ < 30$) and the lowest one is for the pipe center region. Furthermore, it was concluded that the new number

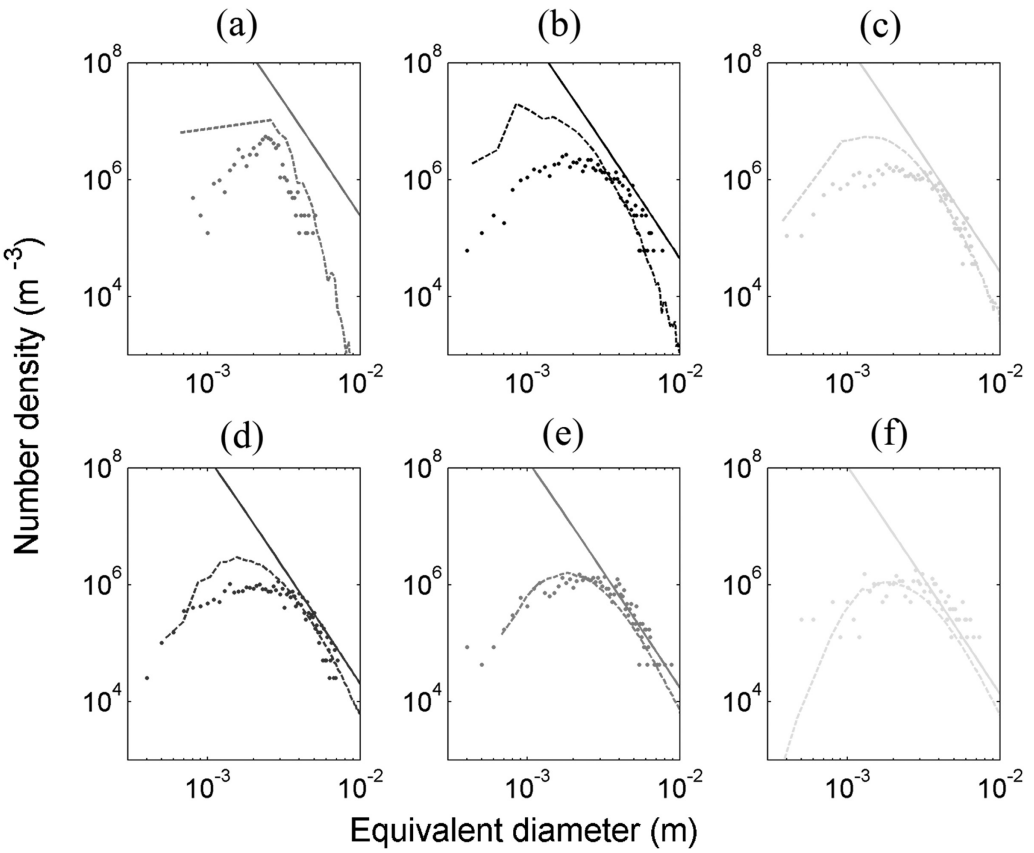

Figure 8. Number density of turbulent vortices at different radial locations.

(a) $0.93 < r/R < 1$; (b) $0.8 < r/R < 0.93$; (c) $0.6 < r/R < 0.8$; (d) $0.4 < r/R < 0.6$; (e) $0.2 < r/R < 0.4$; (f) $0 < r/R < 0.2$. Solid lines represent the old model, dashed lines are the new model and the dots are the quantified number densities. [Color figure can be viewed in the online issue, which is available at wileyonlinelibrary.com.]

density model, particularly in fraction a, predicts the number densities more reliable than the old model.

The average size distributions of vortex cores and regrown vortices identified using the vortex-tracking algorithm with respect to their radial location in the computational domain is shown in Figure 9. The equivalent sphere diameter was considered as the relevant vortex size. It is seen in Figure 9 that the vortex-core size is increasing significantly from near-wall region to the bulk flow of the denser region in the computational domain, and the smallest vortex is located at near-wall region as it is expected. For the regrown vortices, the average size distribution increases marginally from near wall to the bulk flow region. This happens due to the regrowing process of vortex-cores in the vortex-tracking algorithm. As it was mentioned before, the vortex location and its vorticity magnitude are the criteria to regrow the cores. The small vortex cores that mostly are located in the near-wall region tend to regrow with high rate as they have large vorticity magnitudes. Conversely, the number density of vortices in near-wall region is higher. Therefore, there is limited space to grow the vortices in near-wall region.

Conclusions

In this study, the number densities of turbulent vortices for three different subranges of the energy spectrum (dissipation, inertial, and energy containing) were studied, and a new number density model was proposed for the complete energy spectrum. The new model depends on the vortex size, local kinetic energy, and dissipation rate.

A comparison between the old and new number density models shows that the new number density model significantly improved the prediction of the turbulent vortices number density. The new number density model was validated by the number density distribution quantified in the turbulent pipe flow using the 3-D vortex-tracking algorithm which was previously developed by the authors. In the new model, the nondimensional functions f_L and f_η allow the number density distributions to be predicted accurately also for the dissipation and energy containing subranges.

The number densities of turbulent vortices, modeled and quantified, vary at different radial locations. It was also observed that the highest number density was for the near-wall region and the lowest number density is for the pipe center region. Furthermore, the average size distributions of turbulent vortex cores show that the sizes of vortex-cores and regrown vortices increase from near-wall region to the bulk of the flow.

Notation

C = structure function parameter
C_η = constant
C_L = constant
C_μ = constant
E = turbulent energy spectrum, $m^3\ s^{-2}$
f_L = nondimensional function for energy contacting in energy spectrum
f_η = nondimensional function for dissipation subrange in energy spectrum
k = turbulent kinetic energy, $m^2\ s^{-2}$
L = energy containing scale, m
L' = energy containing scale, m
$\dot{n}$ = number density, m^{-3}
P_0 = constant
$\bar{u}$ = mean of fluctuating velocity, $m\ s^{-1}$
y^+ = nondimensional wall distance

Greek letters

α = Kolmogorov constant
β = constant
ε = energy dissipation rate, $m^2\ s^{-3}$
η = Kolmogorov scale, m
κ = wave number, m^{-1}
λ = vortex size, m
υ = kinematic viscosity, $m^2\ s^{-1}$
ρ = density, $kg\ m^{-3}$

Literature Cited

1. Liao Y, Lucas D. A literature review of theoretical models for drop and bubble breakup in turbulent dispersions. *Chem Eng Sci*. 2009; 64(15):3389–3406.
2. Lasheras JC, Eastwood C, Martínez-Bazán C, Montañés JL. A review of statistical models for the break-up of an immiscible fluid immersed into a fully developed turbulent flow. *Int J Multiphase Flow*. 2002;28(2):247–278.
3. Prince MJ, Blanch HW. Bubble coalescence and break-up in air-sparged bubble columns. *AIChE J*. 1990;36(10):1485–1499.
4. Andersson R, Helmi A. Computational fluid dynamics simulation of fluid particle fragmentation in turbulent flows. *Appl Math Model*. 2014;38(17–18):4186–4196.
5. Ghasempour F, Andersson R, Andersson B. Multidimensional turbulence spectra–statistical analysis of turbulent vortices. *Appl Math Model*. 2014;38(17–18):4226–4237.
6. Pope SB. *Turbulence Flows*. Cambridge: Cambridge University Press, 2000.
7. Jakobsen HA. *Chemical Reactor Modeling- Multhiphase Reactive Flows*. Berlin: Springer, 2008.
8. Azbel D, Athanasios IL. *A Mechanism of Liquid Entrainment*. Ann Arbor, MI.: Ann Arbor Sci. Pub., 1983.
9. Dritschel DG. Vortex properties of two-dimensional turbulence. *Phys Fluids A: Fluid Dyn (1989–1993)*. 1993;5(4):984–997.
10. Luo H, Svendsen HF. Theoretical model for drop and bubble breakup in turbulent dispersions. *AIChE J*. 1996;42(5):1225–1233.
11. Han L, Gong S, Li Y, Gao N, Fu J, Luo H, Liu Z. Influence of energy spectrum distribution on drop breakage in turbulent flows. *Chem Eng Sci*. 2014;117:55–70.
12. Batchelor G. *The Theory of Homogenous Turbulence*. Cambridge: Cambridge University of Press, 1982.
13. Martinez-Bazan C, Montanes JL, Lasheras JC. On the breakup of an air bubble injected into a fully developed turbulent flow. Part 1. Breakup frequency. *J Fluid Mech*. 1999;401:157–182.
14. Pope SB. Ten questions concerning the large-eddy simulation of turbulent flows. *New J Phys*. 2004;6:35.
15. Davidson L. Large Eddy simulations: how to evaluate resolution. *Int J Heat Fluid Flow*. 2009;30(5):1016–1025.
16. Ghasempour F, Andersson R, Kevlahan N, Andersson B. Multidimensional turbulence spectra – identifying properties of turbulent structures. J Phys Conf Ser. 2011;318:042022.
17. Andersson B, Andersson R, Håkanssen L, Mortensen M, Sudiyo R, Wachem B. *Computational Fluid Dynamics for Engineers*. Cambridge: Cambridge University Press, 2012.

Manuscript received July 24, 2014, and revision received Aug. 22, 2014.